Università degli studi di Udine

Design and Simulation of a 12 Gb/s Transceiver With 8-Tap FFE, Offset-Compensated Samplers and Fully Adaptive 1-Tap Speculative/3-Tap DFE and

(Article begins on next page)

28 April 2024

Design and Simulation of a 12 Gb/s Transceiver with 8-Tap FFE, Offset-Compensated Samplers and Fully-Adaptive 1-Tap Speculative/3-Tap DFE and Sampling Phase for MIPI A-PHY Applications

Davide Menin[ID], Andrea Bandiziol[ID], Werner Grollitsch, *Member,* IEEE, Roberto Nonis, *Member,* IEEE and Pierpaolo Palestri[ID], *Senior Member,* IEEE

Abstract—**This paper presents a fully-adaptive high-speed serial interface designed in 28 nm planar CMOS technology for future MIPI-compliant automotive microcontrollers operating at 12 Gb/s over long-reach channels. The transmitter has a voltage-mode driver and operates at full rate featuring an 8-tap feed-forward equalizer with tap programmability of 1/16. Transmitter's output impedance tuning is performed through activation of different driver replicas. The half-rate receiver features an analog front-end which comprises a variable-gain amplifier and a continuous-time linear equalizer. The subsequent decision-feedback equalizer has 3 programmable taps, the first of which is loop-unrolled to relax timing constraints. Another amplifier is embedded in the DFE's summing node. We employ transistor-level simulations to assess the capability of the interface to optimally adapt to realistic channels: The DFE taps and the data sampling phase are automatically adapted by means of a behavioural implementation of an LMS algorithm based on information gathered through error sampling. Such an interface was simulated on channels representing likely MIPI A-PHY to-be-defined specifications featuring up to 33 dB loss at 6 GHz.**

Index Terms—**High-Speed Serial Interfaces, Automotive, Inter-Symbol Interference, LMS Adaptive Equalization, MIPI A-PHY**

I. INTRODUCTION

High-speed serial interfaces (HSSI) for chip-to-chip communications are becoming of widespread use in servers, portable devices and many other consumer applications due to the ever-increasing need for high data rates and low energy-per-bit [1]–[3]. In this respect, automotive systems lag behind consumer applications in terms of bit rate, but demand for high-speed interfaces is expected to grow with the advent of Advanced Driving-Assistance Systems [4]–[6], hence requiring complex design techniques to be brought into the automotive environment. Data rates faster than 10 Gb/s are expected to become common in the near future and capable of coping with channels featuring significant attenuation [6], [7]. The resulting inter-symbol interference (ISI) requires aggressive equalization strategies [1], [2], [8], [9]. Due to the change in the channel characteristics over PVT (process, voltage and

D. Menin and P. Palestri are with the Polytechnic Department of Engineering and Architecture (DPIA), University of Udine, 33100 Udine, Italy (e-mail: menin.davide@spes.uniud.it).
A. Bandiziol, W. Grollitsch and R. Nonis are with Infineon Technologies, 9500 Villach, Austria

temperature) variations and to allow the transceiver to operate on largely different channels, equalization parameters need to be tuned by fully-adaptive algorithms [9].

In this paper, through accurate probabilistic models as well as behavioural Verilog-A system-level modelling [10] coupled to post-layout transistor-level simulations, we present the capability of the transceiver in [11] to operate at the increased speed of 12 Gb/s (w.r.t. 9.2 Gb/s of the past implementation) with a channel complying with typical specifications of yet-to-be-defined MIPI A-PHY standard featuring an attenuation of 33 dB at Nyquist frequency [6].

The paper proceeds as follows: section II describes the architecture of the transceiver, the upgrade from the past realization [5], [11], [12] and the tests demonstrating operation over the automotive PVT range; section III describes the implementation of the fully-adaptive algorithm; transistor-level simulations are shown in section IV for realistic automotive channels, with considerations on the transceiver's equalization strategy; conclusions are drawn in section V.

II. TRANSCEIVER ARCHITECTURE

The block diagram of the transceiver is sketched in Fig. 1. In this paper we focus on the adaptive equalization of the channel. Details on the CDR algorithm are reported in [12].

The transmitter [5] operates at full rate and performs feed-forward equalization (FFE) with 1 pre-, 1 main- and 6 post-cursors, all programmable in steps of $1/16$ ($\approx 1.16 \, \text{dB}$ of variation). A low-dropout regulator (LDO) is used to set the output voltage swing. Different replicas of the driver can be connected in parallel to set the transmitter's output impedance.

The receiver [12] operates at half rate with a 1-tap speculative decision-feedback equalizer (DFE) featuring other 2 non-speculative taps, all programmable with steps of 7 mV. A programmable variable gain amplifier (VGA) at the input adapts the voltage swing for the subsequent continuous-time linear equalizer (CTLE). In addition to the architecture presented in [12], Fig. 1 shows two error samplers with variable threshold $dLev$ (other two are in the odd path) used to perform full adaptation as described in the following section.

The circuit was designed in 28 nm planar CMOS technology and experimental data proving operation up to 9.2 Gb/s was
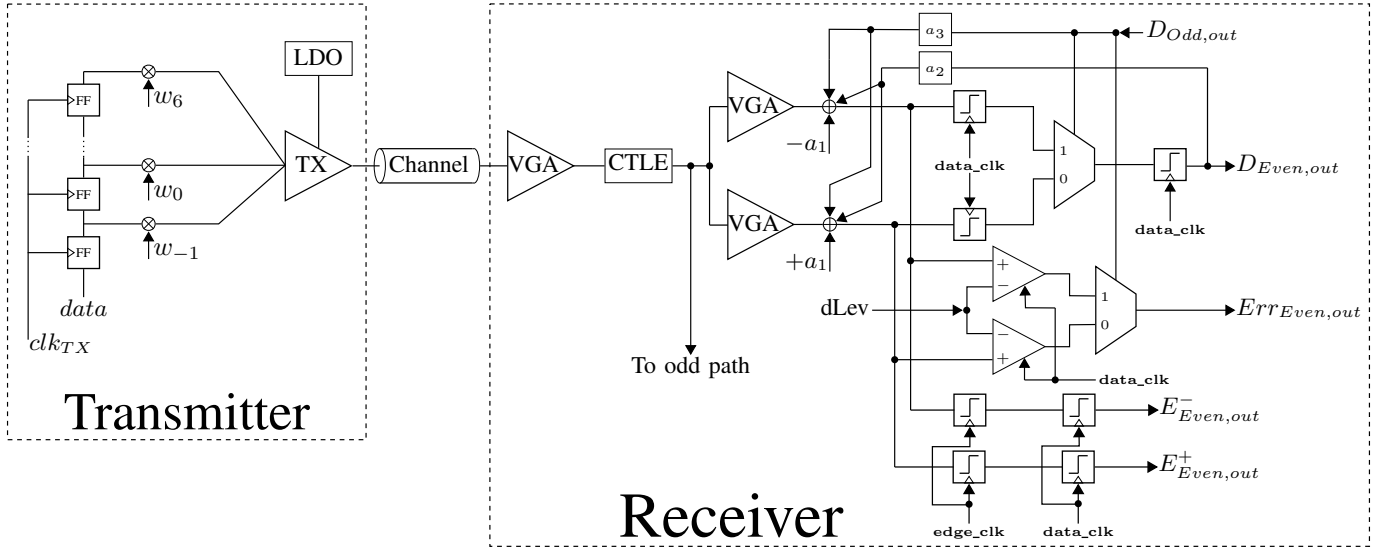
Fig. 1. General architecture of the transceiver (lines are drawn as single-ended although signalling is differential). On the left, the transmitter is shown with FFE; the transmission channel is followed by an analog front-end comprising a VGA and a CTLE stage; the subsequent even portion of the half-rate receiver (the odd portion is omitted for simplicity) on the right implements a 3-tap speculative DFE; edge and error sampling is shown on the bottom right. The CDR provides the edge clock, while the adaptive block (not shown) computes the DFE taps, $dLev$ and the skew between the edge and data clocks.

reported in [11]. Parts of the circuit have been re-designed to increase the speed up to 13 Gb/s: Most notably, now the receiver's CTLE and VGAs are capable of compensating 7.5 dB and 6 dB, respectively, and one of the DFE taps has been detached in order to implement offset compensation at the samplers at start-up time; other components were optimized for such a higher speed. As a consequence, the transceiver's figure of merit reported in [11] has increased to 6.8 mW/Gb/s w.r.t. 5.7 mW/Gb/s in Table I therein. Simulations (see Table I here) demonstrate operation of the transmitter up to 12 Gb/s over the whole automotive range of temperature (−40 °C to 150 °C), supply (−10 % to +10 %) and technology corners (only slow-slow and fast-fast results are reported for brevity). We simulated the whole transceiver in loopback mode and found no errors in the received ∼ 2^{15} bits over the whole automotive PVT range. Longer mixed-signal simulations on XA-VCS showed no errors.

III. ADAPTATION ALGORITHM

Implementation of fully-adaptive algorithms requires additional hardware with respect to the receiver described in [12]. We added the error samplers shown in Fig. 1 that compare the equalized received analog data with the *data level dLev* [13]. Error and data samples are deserialized 1:40 and then input to the LMS algorithm [9]. The LMS loop for $dLev$ is updated based on the correlation between data and error samples:

$$dLev^{new} = dLev^{old} + \Delta_{dLev} \frac{1}{N} \sum_{i=1}^{N} d_i e_i \qquad (1)$$

where d_i and e_i are the i-th received data and edge samples, respectively, $\Delta_{dLev} = 60$ mV, $N = 80$ bit sequence length.

The j-th DFE tap is updated, with $\Delta_{DFE} = 40$ mV, as

$$a_j^{new} = a_j^{old} + \Delta_{DFE} \frac{1}{N-j} \sum_{i=1}^{N-j} d_{i-j} e_i \qquad (2)$$

TABLE I
SIMULATED EYE HEIGHT (EH) AND WIDTH (EW) FOR AUTOMOTIVE CORNERS AT 12 Gb/s. SUPPLY PARASITICS: R = 1 Ω AND L = 1 nH; GROUND PARASITICS: R = 200 mΩ AND L = 200 pH.

	Corners		Figures of merit	
Voltage [%]	Temperature [°C]	Technology	EH [mV]	EW [ps]
10	150	FF	596	75
10	150	SS	487	74
10	−40	FF	626	76
10	−40	SS	505	81
−10	150	FF	556	76
−10	150	SS	436	73
−10	−40	FF	549	75
−10	−40	SS	438	73

The optimal sampling point is found through another LMS loop that modifies the data-sampling phase w.r.t. the edge-sampling clock determined by the CDR [9]:

$$\phi^{new} = \phi^{old} - \Delta_\phi \frac{1}{N-1} \sum_{i=1}^{N-1} d_{i-1} e_i \qquad (3)$$

where ϕ is the shift w.r.t. the CDR edge clock, $\Delta_\phi = 27°$.

The FFE and CTLE parameters are implemented as *pre-settings*, as adaptation of the former would require a back-channel [13], while our implementation of the latter has a quite coarse graining that is not well suited for adaptation.

At this stage of system development, the error samplers and the DAC producing $dLev$ are implemented in a behavioural Verilog-A block to test the performance of the algorithm.

IV. RESULTS

In this section we simulated the performance of the transceiver and of the fully-adaptive algorithm considering a channel likely compliant with future definition of the MIPI
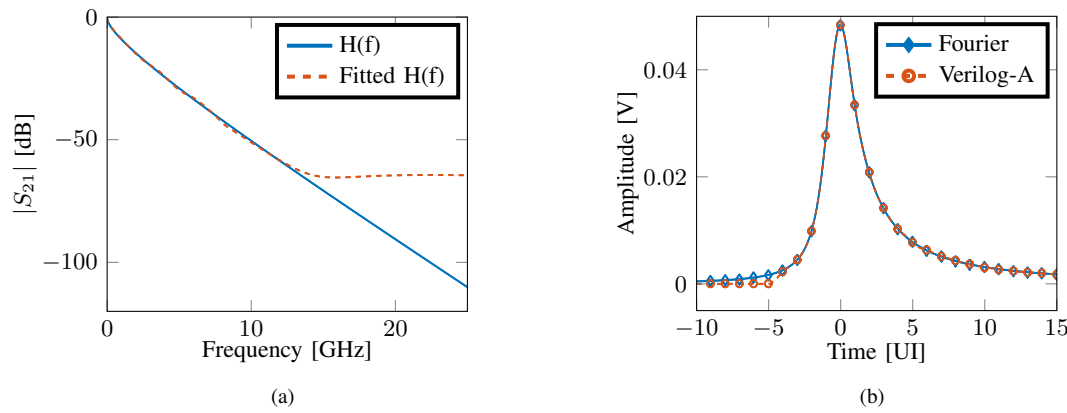
Fig. 2. (a) Insertion loss and (b) pulse responses of a channel targeted by MIPI A-PHY applications having 33 dB loss at 6 GHz. The solid line is obtained with the full microstrip model, the dashed line is the response to its rational fit (4). All equalizers and amplifiers are turned off.
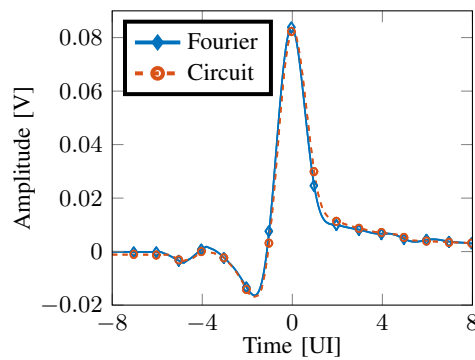

Fig. 3. Pulse response obtained from the fitted MIPI A-PHY channel of Fig. 2(a) with an FFE pre-set of $w_{-1} = -4/16$, $w_0 = 9/16$, $w_1 = -3/16$, and with the CTLE and the two VGAs amplifying respectively 4 dB and 5.5 dB at Nyquist frequency. The solid line is the anti-transform of the transfer function in Eq. (4) convolved with the transmitted pulse, while the dashed line is plotted from transistor-level simulations.
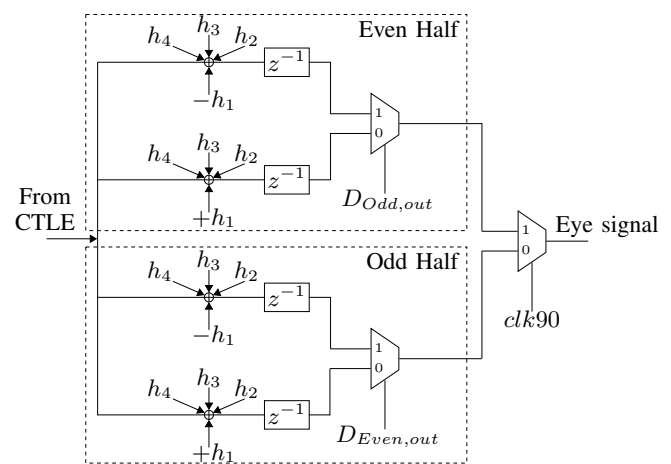

Fig. 4. Schematic of the virtual eye monitor that allows to visualize the effect of the full DFE, despite the first tap being speculative. All multiplexers and delays are behavioural blocks of analog circuits.

A-PHY standard. Since S parameters of such a channel will be available only at the end of 2019, we worked with a well-established procedure [10] and translated the projected loss of such a channel in a microstrip structure losing roughly 33 dB at Nyquist frequency. The channel is modelled numerically in the following way. Firstly, the characteristic impedance and effective dielectric constant are related to the microstrip geometry according to [14]. Secondly, RLCG parameters are extracted and combined with the driver and receiver impedance in order to compute the channel's transfer function [15]. We selected a geometry giving a single-ended impedance of 50 Ω up to 12 GHz. We then tweaked the microstrip's parameters in order to obtain an attenuation of 33 dB at 6 GHz, which is expected to be the typical loss MIPI A-PHY and IEEE 802.3 are currently targeting [7], [16], [17]. The resulting gain as a function of frequency is reported in Fig. 2(a).

The channel is included in the circuit simulations as a rational function fitted to the analytical model [3] as

$$H(s) = \left(\sum_{l=1}^{M} \frac{B_l}{s - A_l} + C \right) e^{-sD} \qquad (4)$$

The transfer function resulting from such a fit is shown by

the red dashed line in Fig. 2(a). In Fig. 2(b), the resulting pulse response is compared to the one produced by Fourier anti-trasformation of the complete transfer function convolved with the transmitted pulse using the method presented in [18].

The channel features many post-cursors and two large pre-cursors. The peak is significantly attenuated to approximately 50 mV, while the transmitted differential swing was 0.6 V. The corresponding simulated eye diagram (not shown) is completely closed and corresponds to a very high BER. In such a situation, DFE alone cannot compensate ISI since its feedback register always contains wrong bit decisions. We thus adjusted the system's pre-set (VGAs, CTLE and FFE) to improve the reception. Those need not be optimal settings, and may be determined in a calibration procedure prior to the beginning of transmission. In fact, it will be shown later on that the same pre-settings can be suited also as starting point for different channels, thus demonstrating that they do not need to be chosen precisely. The resulting pulse response is reported in Fig. 3: The cursors are greatly reduced, although the eye diagram is still closed, despite the action of the analog front-end (amplifying ≈ 15 dB at Nyquist frequency).
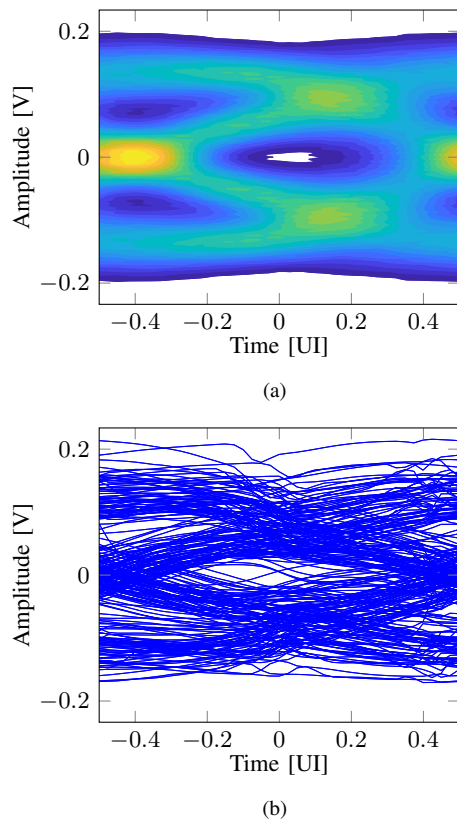
(a)

(b)

Fig. 5. Eye diagram corresponding to the pulse response of Fig. 3 (before adaptive equalization). On the left, (a) was constructed from the pulse response by using a newly-developed probabilistic algorithm [15]; on the right, (b) was obtained through transistor-level simulations.
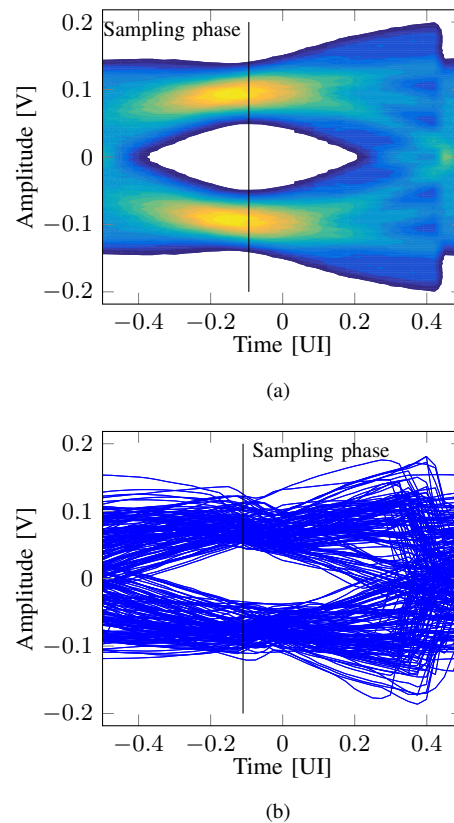

(a)

(b)

Fig. 7. Eye diagrams after convergence of the LMS equalization loops on the channel of Fig. 2(a) as obtained through (a) post-processing of the pulse response with the method in [15] and (b) transistor-level simulations.
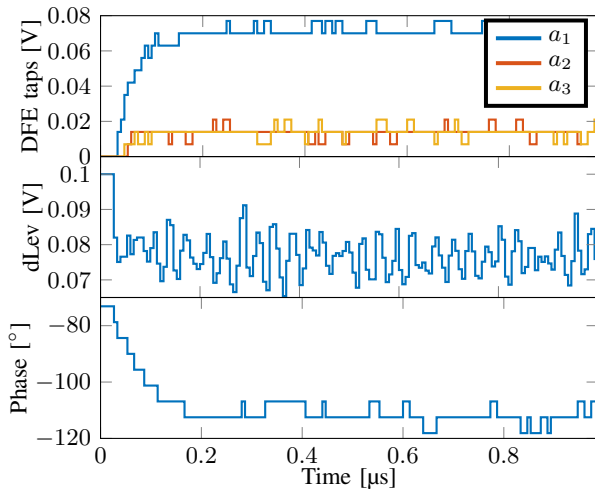

Fig. 6. Equalization quantities adapted by the behavioural block as a function of time as obtained from transistor-level simulation. The DFE taps and the phase are computed as digital codes and were converted to physical quantities for plotting purposes.

Obtaining the eye diagram from the circuit simulation is not straightforward. The receiver is half rate and the DFE is speculative: There are 4 analog nodes connected to 4 samplers (Fig. 1). For plotting purposes, we added behavioural analog multiplexers to combine these 4 signals and plot a single eye diagram taking into account the speculative tap (Fig. 4).

For the MIPI A-PHY channel with the pre-set of Fig. 3 we obtained the eye in Fig. 5(b), which is so closed as in Fig. 5(a) (obtained from post-processing of the pulse response [15]).

DFE and optimal sampling point adaptation are needed in order to improve the situation. The convergence of the LMS loops based on Eqs. (1), (2) and (3) is reported in Fig. 6. $dLev$ converges in the proximity of 80 mV, roughly corresponding to the peak in Fig. 3. The optimal sampling point moves to about 70° away from the edge clock phase (compared to the 90° commonly set by the CDR to have the sampling phase exactly between the transition edges). The 3 DFE taps converge to 70 mV, 14 mV and 14 mV respectively, similarly to the post-cursors in Fig. 3 after the sampling point is moved towards the left (to reduce the first pre-cursor).

The eye diagrams after full adaptation, i.e. obtained by post-processing the pulse response of Fig. 3 after DFE and sampling point adaptation and from transistor-level simulations, are reported in Fig. 7: We now observe an open eye that proves the correctness of the adaptive loop for DFE and optimal sampling point. This is also supported by the null bit-error rate in the circuit simulation after a sequence of 10^4 bits. We also see that the circuit simulation is in good agreement with the eye obtained via numerical elaboration of the pulse response [15]. Although the time-domain transistor-level simulations cannot prove functioning with BER $< 10^{-12}$ (as required by MIPI A-PHY and IEEE 802.3), the post-processing of the pulse response suggests that this
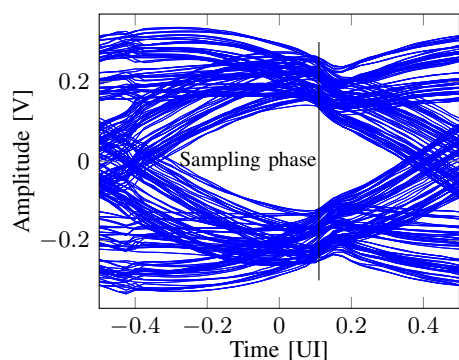
Fig. 8. Eye diagram after convergence of the LMS equalization loops on a channel with 20 dB loss at 6 GHz as obtained from transistor-level simulation.

is the case, provided that the jitter of the clock and CDR is sufficiently low. To have a rough estimate of the effect of jitter, we exploit the method in [19] applied to the eye obtained from post-processing of the pulse response. The jitter is estimated to be 1.5 ps RMS from the bathtub plots measured at 4.6 Gb/s in [11] and scaled to 12 Gb/s operation using a simple theoretical model; the result is a reduction in eye width from ≈ 38 ps to ≈ 19 ps at BER $= 10^{-12}$.

We now show that the FFE, CTLE and VGAs pre-sets chosen above can support fully-adaptive operations for different channels. We chose a channel with the same geometry and physical characteristics as the one in Fig. 2(a), now attenuating 20 dB at Nyquist frequency. The equalised eye diagram is shown in Fig. 8, demonstrating equalization capabilities over different channels. Differently from Fig. 7, now the optimal sampling point is delayed with respect to the center of the eye, because the chosen FFE pre-set results in a negative pre-cursor, which is compensated by moving the sampling point to the right (in the previous case it was moved to the left).

V. CONCLUSIONS

We have devised an accurate modelling procedure based on probabilistic system-level calculations and behavioural models coupled to transistor-level simulations to show the capability of a HSSI operating at 12 Gb/s to properly equalize channels with a wide range of attenuation from 20 dB to 33 dB at 6 GHz and to operate over the whole automotive PVT range. We have proven that a single pre-set for FFE and CTLE can work with different channels: If the attenuation is low, the pre-set over-compensates the pre- and post-cursor, but adaptive DFE and optimal sampling point counteract this effect.

Through efficient probabilistic post-processing of the pulse response [15] we have also shown how to estimate eye diagrams which closely resemble the time-domain transistor-level simulations, which is useful to estimate the BER.

Overall, such a coupled circuit/behavioural modelling approach proved to be a powerful tool to determine the performance of high-speed serial interfaces and provide guidelines about equalization and LMS parameters.

ACKNOWLEDGEMENTS

REFERENCES

[1] T. C. Carusone, "Introduction to Digital I/O: Constraining I/O Power Consumption in High-Performance Systems," *IEEE Solid-State Circuits Mag.*, vol. 7, no. 4, pp. 14–22, Fall 2015.

[2] J. Lee, K. Park, K. Lee, and D.-K. Jeong, "A 2.44-pJ/b 1.62–10-Gb/s Receiver for Next Generation Video Interface Equalizing 23-dB Loss With Adaptive 2-Tap Data DFE and 1-Tap Edge DFE," *IEEE Trans. Circuits Syst. II*, vol. 65, no. 10, pp. 1295–1299, Oct. 2018.

[3] J. Park, J.-H. Chae, Y.-U. Jeong, J.-W. Lee, and S. Kim, "A 2.1-Gb/s 12-Channel Transmitter With Phase Emphasis Embedded Serializer for 55-in UHD Intra-Panel Interface," *IEEE J. Solid-State Circuits*, vol. 53, no. 10, pp. 2878–2888, Oct. 2018.

[4] N. J. Endo, "Wireless Communication In and Around the Car: Status and Outlook. ES3: High-Speed Communications on 4 Wheels: What's in Your next Car?" in *2013 IEEE Int. Solid-State Circuits Conf. Dig. of Tech. Papers*, Feb. 2013, pp. 515–515.

[5] A. Bandiziol, W. Grollitsch, F. Brandonisio, R. Nonis, and P. Palestri, "Design of a 8-taps, 10gbps transmitter for automotive microcontrollers," in *2016 IEEE Asia Pacific Conf. on Circuits and Syst. (APCCAS)*, Oct 2016, pp. 321–324.

[6] "IEEE P802.3ch Multi-Gig Automotive Ethernet PHY Task Force," http://www.ieee802.org/3/ch/public/mar18/index.html, Mar. 2018.

[7] E. Di Biaso, B. Bergner, and C. Mandel, "High Speed Channel Modeling and Analysis," Apr. 2018. [Online]. Available: http://www.ieee802.org/3/ch/public/adhoc/Bergner_DiBiaso_Mandel_3ch_01_0418.pdf

[8] J. F. Bulzacchelli, "Equalization for Electrical Links: Current Design Techniques and Future Directions," *IEEE Solid-State Circuits Mag.*, vol. 7, no. 4, pp. 23–31, Fall 2015.

[9] V. Balan, O. Oluwole, G. Kodani, C. Zhong, R. Dadi, A. Amin, A. Ragab, and M.-J. E. Lee, "A 15–22 Gbps Serial Link in 28 nm CMOS With Direct DFE," *IEEE J. Solid-State Circuits*, vol. 49, no. 12, pp. 3104–3115, 2014.

[10] D. Menin, A. De Prà, A. Bandiziol, W. Grollitsch, R. Nonis, and P. Palestri, "A Simple Simulation Approach for the Estimation of Convergence and Performance of Fully-Adaptive Equalization in High-Speed Serial Interfaces," *IEEE Trans. Compon. Packag. Manuf. Technol.*, 2019, available online.

[11] A. Bandiziol, W. Grollitsch, G. Steffan, R. Nonis, and P. Palestri, "Design and Characterization of a 9.2-Gb/s Transceiver for Automotive Microcontroller Applications With 8-Taps FFE and 1-Tap Unrolled/4-Taps DFE," *IEEE Trans. Circuits Syst. II*, vol. 65, no. 10, pp. 1305–1309, Oct. 2018.

[12] A. Bandiziol, W. Grollitsch, F. Brandonisio, M. Bassi, R. Nonis, and P. Palestri, "Design of a Half-Rate Receiver for a 10Gbps Automotive Serial Interface with 1-Tap-Unrolled 4-Taps DFE and Custom CDR Algorithm," in *2018 IEEE Int. Symp. on Circuits and Syst. (ISCAS)*, May 2018, pp. 1–5.

[13] V. Stojanović, A. Ho, B. Garlepp, F. Chen, J. Wei, G. Tsang, E. Alon, R. Kollipara, C. Werner, J. Zerbe, and M. Horowitz, "Autonomous dual-mode (PAM2/4) serial link transceiver with adaptive equalization and data recovery," *IEEE J. Solid-State Circuits*, vol. 40, no. 4, pp. 1012–1026, Apr. 2005.

[14] M. Dazzi, P. Palestri, D. Rossi, A. Bandiziol, I. Loi, D. Bellasi, and L. Benini, "Sub-mW multi-Gbps chip-to-chip communication Links for Ultra-Low Power IoT end-nodes," in *2018 IEEE Int. Symp. on Circuits and Syst. (ISCAS)*, May 2018, pp. 1–5.

[15] A. Cortiula, M. Dazzi, M. Marcon, D. Menin, A. Bandiziol, A. Cristofoli, W. Grollitsch, R. Nonis, and P. Palestri, "A Simple and Fast Tool for the Modelling of Inter-Symbol Interference and Equalization in High-Speed Chip-to-Chip Interfaces," in *The 42nd Int. Conv. on Information and Communication Technol., Electronics and Microelectronics (MIPRO)*, May 2019.

[16] T. Müller, "802.3ch channel measurement results," Oct. 2017. [Online]. Available: http://www.ieee802.org/3/ch/public/adhoc/2017-10-04%20802.3ch%20channel%20measurementresults%20.pdf

[17] E. Di Biaso, "Insertion Loss Limit Analysis," May 2018. [Online]. Available: http://www.ieee802.org/3/ch/public/adhoc/DiBiaso_3ch_01_05-30-18%20-%20adhoc.pdf

[18] T. Brazil, "Causal-convolution – a new method for the transient analysis of linear systems at microwave frequencies," *IEEE Trans. Microw. Theory Techn.*, vol. 43, no. 2, pp. 315–323, Feb. 1995.

[19] A. Sanders, "Statistical Simulation of Physical Transmission Media," *IEEE Trans. Adv. Packag.*, vol. 32, no. 2, pp. 260–267, May 2009.